PAPER

Check for updates

Reactive adsorption desulfurization of NiO and Ni^0 over NiO/ZnO–Al$_2$O$_3$–SiO$_2$ adsorbents: role of hydrogen pretreatment

Feng Ju,[a] Miao Wang, [a] Hui Luan,[ab] Pengyu Du,[c] Zhihe Tang[b] and Hao Ling*[a]

Reactive adsorption desulfurization (RADS) of Fluidized Catalytically Cracked (FCC) gasoline on reduced and unreduced NiO/ZnO–Al$_2$O$_3$–SiO$_2$ adsorbents was studied. Various characterizations such as powder X-ray diffraction (XRD), H$_2$-temperature-programmed reduction (H$_2$-TPR), the H$_2$/O$_2$ pulse titration (HOPT), transmission electron microscopy (TEM) and X-ray photoelectron spectroscopy (XPS) are used to evaluate the effects of hydrogen pretreatment of the adsorbents. XRD and HOPT results indicate that NiO is hard to be reduced to Ni^0 under the conditions of RADS. H$_2$-TPR shows that NiO might be reduced to Ni^0 at the temperature of 598 °C, much higher than the temperature of RADS. The Ni 2p$_{3/2}$ spectrum of Ni^0 is not observed for the reduced adsorbent, but the main peak of Ni 2p$_{3/2}$ of NiS is found for the spent adsorbent. The unreduced NiO/ZnO–Al$_2$O$_3$–SiO$_2$ adsorbent performs a better desulfurization than the reduced adsorbent at the beginning of desulfurization process. NiO and Ni^0 are assumed as the main active components and present a good desulfurization ability in RADS. Finally, a change in the RADS mechanism is presented and discussed.

Introduction

Deep desulfurization of fossil oil is one of the most urgent and challenging tasks due to the stringent environmental legislations. Compared to the conventional hydrodesulfurization process, reactive adsorption desulfurization (RADS), as a new desulfurization process, could save the cost of hydrogen and reduce the loss of octane number.[1,2] The commercial S-Zorb process developed by Conoco Philips Petroleum Co. is an effective RADS method for producing ultralow sulfur gasoline and diesel.[3–6] In the RADS process, the active component Ni is regarded as important in the selective adsorption of sulfur atoms. Sulfur atoms of sulfur-containing molecules adsorb onto the adsorbents first, and then react with the adsorbents.[7] The hydro-carbon portion of the molecule is released back into the product stream.

Tawara et al. first investigated conventional HDS catalyst in the adsorptive HDS of kerosene, and found that the desulfurization performance of the oxidized Ni–Mo/Al$_2$O$_3$ catalyst was better than that of the sulfide Ni–Mo/Al$_2$O$_3$ catalyst.[8] They used ZnO species as the catalyst supporter and found that the ZnO particles could adsorb the H$_2$S which released from NiS by hydrogen. After that, Babich and Moulijin presented a RADS

mechanism.[9] They discovered that nickel selected and reacted with sulfur atom under hydrogen to form NiS, which consequently reacted with neighbouring ZnO to form ZnS and regenerated nickel.

The mechanism and operating conditions of RADS over Ni/ZnO-based adsorbent has been attracted more attention in recent studies.[10–17] Bezverkhyy et al. studied the kinetics of thiophene reactive adsorption on Ni/ZnO.[18,19] Their results indicated that the reaction between Ni/ZnO and thiophene consists of three steps. The first step is a rapid surface reaction between thiophene and the surface Ni atom to form Ni$_3$S$_2$. The next step is sulfur species reacting preferably with ZnO. The third step is thiophene molecules reacting with bulk Ni atoms, meanwhile H$_2$S diffuses through ZnS layer to react with bulk ZnO. Zhang et al.[20] reported the effect of ZnO particle size on the adsorptive desulfurization performance for Ni/ZnO adsorbent.[20] The desulfurization activity and sulfur capacity of Ni/ZnO adsorbent with smaller ZnO particle sizes are much higher than that with larger sizes.

Normally, hydrogen pretreatment has been taken to reduce the NiO/ZnO-based sorbent to Ni/ZnO-based sorbent before the desulfurization process. Many studies confirmed that reduced Ni is the main active component interacting with sulfur atom.[21,22] However, there are few reports investigating the effect of hydrogen pretreatment on the RADS adsorbent, nor whether NiO could be the main active component for desulfurization. Bezverkhyy et al. compared the desulfurization performance of reduced Ni/ZnO adsorbent and unreduced NiO/ZnO.[19] They found that NiO/ZnO adsorbents can be used in the reactive ad-

[a] State Key Laboratory of Chemical Engineering, East China University of Science and Technology, Shanghai 200237, China. E-mail: linghao@ecust.edu.cn

[b] Research Institute of Safty & Environment Technology, China National Petroleum Corporation, Beijing 102206, China

[c] Petrochina Karamay Petrochemical Co. Ltd., Karamay, Xinjiang 834000, China

sorption of thiophene without any reductive pretreatment. Moreover, the reduction of NiO/ZnO resulted in the formation of Ni–Zn alloyed particles and led to a decrease of the sulfidation rate in comparison with the unreduced sample. In our previous works the effects of dispersion of Ni species and acidity of adsorbent surface on the desulfurization of NiO/ZnO–Al$_2$O$_3$–SiO$_2$ sorbents were discussed.[23,24] It was noticed that hydrogen pre-treatment had little effect on desulfurization. In this work, reduced and unreduced NiO/ZnO–Al$_2$O$_3$–SiO$_2$ adsorbents have been prepared to verify whether hydrogen pretreatment contributes to the desulfurization process. At last, some change of the RADS mechanism on NiO/ZnO–Al$_2$O$_3$–SiO$_2$ adsorbent is discussed.

Experimental section

Adsorbent preparation and feedstock properties

All chemicals used for preparation of the adsorbent were of analytical grade. The feedstock employed in the work was supplied by Petrochina Jilin Petrochemical Company, and its properties are listed in Table 1.

The supporter ZnO–Al$_2$O$_3$–SiO$_2$ of adsorbent was prepared by coprecipitation method, and then Ni component was loaded on the supporter by impregnation method, shown in Fig. 1. A mixed aqueous solution of Al(NO$_3$)$_3$ and Zn(NO$_3$)$_2$ was dropwise added into a mixed solution of Na$_2$CO$_3$(0.2 mol L^{-1}) and Na$_2$SiO$_3$(0.2 mol L^{-1}) at a rate of 15 mL min^{-1} at a precipitation temperature of 20 °C, followed by aging at the same temperature for 2 h. Then, the precipitation was filtrated out and washed with a large quantity of deionized water to remove the residue sodium until the pH of the suspension is below 6.5.[25–28] After that, the filter cake was dried at 120 °C in air for 12 h, and then calcined at 500 °C in a muffle furnace in dry air for 4 h. The supporter ZnO–Al$_2$O$_3$–SiO$_2$ was obtained.

Solutions with Ni(NO$_3$)$_2$ were mixed with the above supporter and stirred for 2 h. After that, a solution of Na$_2$CO$_3$(0.2 mol L^{-1}) was added dropwise into the mixed solution. The precipitation is the precursor of the sorbent. Large amount of deionized water was used to wash away the residue sodium until the pH of the solution is below 6.5. The obtained filter cake was dried at 120 °C in a vacuum oven for 12 h, and then calcined at 500 °C in a muffle furnace for 2 h. Finally, the adsorbent was screened to 120 mesh and kept in a sealed bag before usage.

Desulfurization experiments

The desulfurization experiments were conducted in a continuous micro fixed-bed reactor.[23,24] A total of 3 grams of adsorbent in the oxidized form was loaded into the reactor per run. Before the reaction, the oxidized form sorbent was reduced by
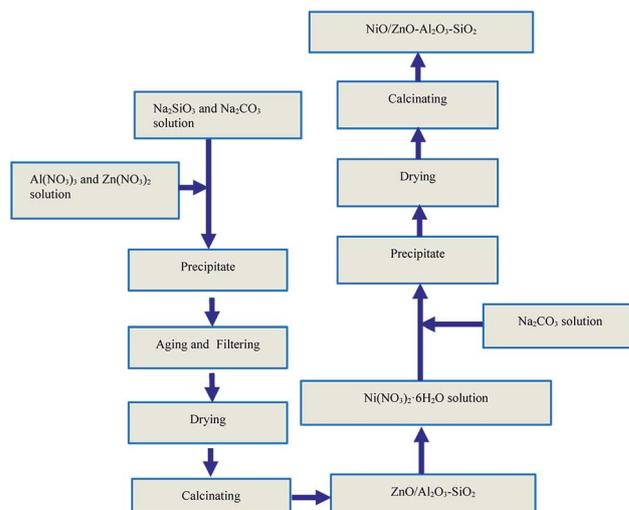

Fig. 1 Preparation process of the NiO/ZnO–Al$_2$O$_3$–SiO$_2$ adsorbent.

hydrogen at a flow rate of 140 mL min^{-1} under 2.0 MPa and 440 °C for 2 h. Then the FCC gasoline was pumped into the reactor. The desulfurization products were collected periodically in a beaker to analyze sulfur content. After desulfurization, an oxide gas containing 2% O$_2$ diluted by 98% N$_2$ was used to regenerate adsorbents and the tail gas was collected by a 0.1 mol L^{-1} NaOH solution each hour. The experimental conditions are listed in Table 2.

The sulfur removal efficiency of adsorbent is defined according to the following equation:[29]

$$R_s(\%) = \frac{C_0 - C_t}{C_0} \times 100 \tag{1}$$

where R_s is the sulfur removal efficiency of the sulfur compounds in the fuel (%), C_0 is the sulfur content of the gasoline feed-stock (μg g^{-1}), C_t is the sulfur concentration of the outlet product at any time (μg g^{-1}).

The breakthrough sulfur capacity is determined as follows.

$$q_{breakthrough} = \frac{\nu C_1}{1000m} \int_0^t R dt \tag{2}$$

where $q_{breakthrough}$ is the breakthrough sulfur capacity of the adsorbent(mg g^{-1}), ν is the feed volumetric flow rate (mL min^{-1}), C_1 is the initial sulfur content in the fuel (mg L^{-1}), m is the weight of the adsorbent (g).[30] The breakthrough time is defined as the RADS time when the sulfur concentration of effluent desulfurized gasoline exceeded 10 μg g^{-1}.

Characterization of adsorbents

The sulfur concentrations of various samples are analyzed by an Antek 9000 total sulfur analyzer.

The crystalline structures of the adsorbents were characterized through X-ray diffraction (XRD) by using a Bruker D8 Advance X-ray diffractometer with a Cu Kα = 0.154 nm monochromatized radiation source, operating at 40 kV and 100 mA.

The crystal lattice of the adsorbents was surveyed by JEM-2100 transmission electron microscope (TEM).

Table 1 Properties of the FCC gasoline

Density (20 °C) g cm^{-3}	Sulfur content μg g^{-1}	Nitrogen content μg g^{-1}
0.723	243.48	28.22

Table 2 Experimental conditions of desulfurization process

Reduction	Temp./°C	440
	Hydrogen pressure/MPa	2.0
	Reduction time/h	2
Adsorption, desulfurization	Temp./°C	419
	Hydrogen pressure/MPa	2.9
	Weight hourly space velocity (MHSV)/h^{-1}	10.84
	Mole ratio (H$_2$/oil)	0.3
	H$_2$ volume/gasoline weight (mL g^{-1})	90
Purge	Temp./°C	360
	H$_2$ flow (mL min^{-1})	200
	Purge time/min	20
Regeneration	Temp./°C	360 480
	Regeneration time/min	30 60
	Total pressure/MPa	0.15
	Oxygen pressure/KPa	3.0
	Flow (mL min^{-1})	200

Fig. 3 H$_2$-TPR of NiO/ZnO–Al$_2$O$_3$–SiO$_2$ adsorbent.

The dispersity and reducibility of Nickel were undertaken by using the H$_2$/O$_2$ pulse titration (HOPT) with a chemisorption analyzer Autochem II 2920(Micromeritics, USA).

Temperature programmed reduction (TPR) was surveyed by the analyzer Autochem II 2920(Micromeritics, USA).

X-ray photoelectron spectroscopy (XPS) was characterized by the multi-function photoelectron spectrometer (ESCALAB 250Xi).

Results and discussion

XRD results

To compare the changes in the lattice before and after reduction, the XRD patterns of adsorbents are shown in Fig. 2. The XRD pattern appears distinguishable characteristic diffract-ion peaks. These peaks are attributed to the crystalline phases of ZnO (2θ = 31.5°, 34.4°, 36.2°, 56.5°, 63°, 68°) and NiO (2θ = 43.3°, 75°). The crystalline phases of Al$_2$O$_3$ and SiO$_2$ cannot be detected.

Fig. 2 XRD images of NiO/ZnO–Al$_2$O$_3$–SiO$_2$ adsorbents before and after reduction.

After reduction, the height of peaks of ZnO (2θ = 36.2°, 63°) decrease and peak width broaden. However, the characteristic diffraction peak of NiO (2θ = 43.3°) become sharp and strong, which means hydrogen reduction affects the lattice of the NiO and ZnO. Hydrogen reduction makes the crystal of NiO become bigger and promotes the dispersion of Zn. The purpose of hydrogen pretreatment is to obtain reduced Ni^0 before the desulfurization process. However, the reduced Ni^0 cannot be detected by XRD, which means that the Ni component is diffi-cult to be reduced in the form of NiO under 440 °C.

TPR results

The H$_2$-TPR method is used to evaluate the reducibility of NiO/ZnO–Al$_2$O$_3$–SiO$_2$ adsorbents, shown in Fig. 3. The adsorbent only shows one hydrogen consumption peak, and this peak is attributed to the reduction of NiO. The characteristic peak loc-ates at 598 °C, however, the reduction temperature is around 440 °C during the RADS process, which is far away from 598 °C.

Shamskar et al. studied the reduction ability of NiO–Al$_2$O$_3$ catalyst.[30] They prepared some NiO–Al$_2$O$_3$ catalysts with different calcination temperature (600–900 °C), and they found the reduction temperature increased with the calcination temperature increasing. The reduction temperature of NiO–Al$_2$O$_3$ catalyst under 600 °C calcination temperature is over 700 °C. This result is consistent with NiO/ZnO–Al$_2$O$_3$–SiO$_2$ adsorbents, whose calcination temperature is 500 °C and reduction temperature is about 600 °C. According to Tang's research, the strong metal-support interactions (SMSI) between Ni and ZnO particles of Ni/ZnO could increase the reduction temperature of NiO in NiO/ZnO to 370 °C, indicating that there exists a strong interaction between NiO and the supporter making NiO much harder to be reduced.[31]

Fig. 4 shows the XRD patterns of adsorbents reduced in H$_2$ for 3 h at 440 °C and 600 °C, respectively. There are two distinguished characteristic diffraction peaks at 2θ = 43.9° and 51.7°, attributed to AlNi$_3$. The ZnO peaks of the adsorbent reduced at 600 °C become sharper and stronger than those of the adsorbent reduced at 440 °C. Under high reduction
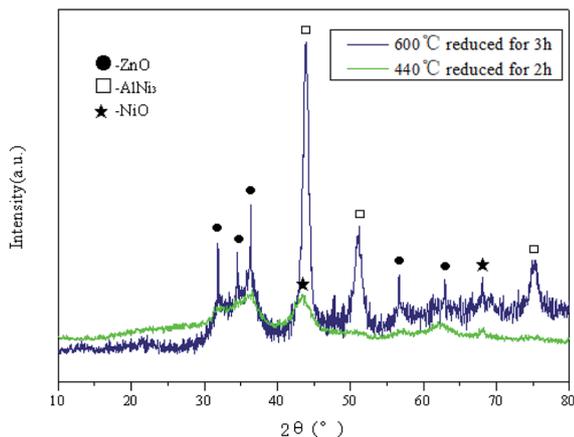
Fig. 4 XRD images of NiO/ZnO–Al$_2$O$_3$–SiO$_2$ adsorbents under different reduction temperature.
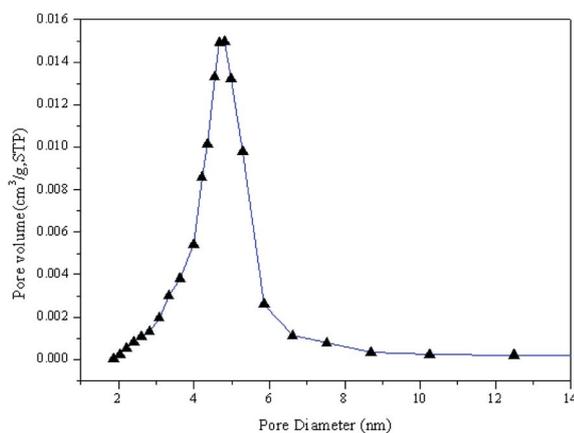

Fig. 5 Pore size distributions of NiO/ZnO–Al$_2$O$_3$–SiO$_2$ adsorbents.

temperature, the crystal of ZnO grows bigger, but NiO is still not reduced to Ni^0. Fig. 4 shows that NiO reacts with Al$_2$O$_3$ to form Ni–Al alloy. In NiO/ZnO adsorbents, hydrogen pretreatment leads to form the Ni–Zn allo-y, while, Ni–Zn alloy cannot be detected in NiO/ZnO–Al$_2$O$_3$–SiO$_2$ adsorbent by XRD.[19] Combined with H$_2$-TPR results, it can be concluded that hydrogen reduces NiO and Al$_2$O$_3$ to form the Ni–Al alloy at 600 °C. The interactions between active component Ni and the supporter are strong. The existence of Al$_2$O$_3$ and ZnO supporter increases the reduction temperature of NiO.

Surface area and pore size distribution

According to the principle of the adsorbents, the adsorption capacity depends on its specific surface area and pore size. The small pore sizes might limit the adsorption of the large sulfur molecular into the adsorbent pores. Fig. 5 shows the pore size distribution of the sorbent. Table 3 shows the specific surf-ace areas, pore volume and pore diameter of the adsorbent. It can be seen the pore size diameter ranges from 2.5 to 5.5 nm. These large pores are formed because of the sintering of relatively small pores under high calcination temperatures.[24]

Table 3 Textural properties of adsorbents

S_{BET} (m^2 g^{-1})	V_{total} (cm^3 g^{-1})	DA (nm)
149.01	0.33	5.90

Table 4 Ni dispersion of adsorbents

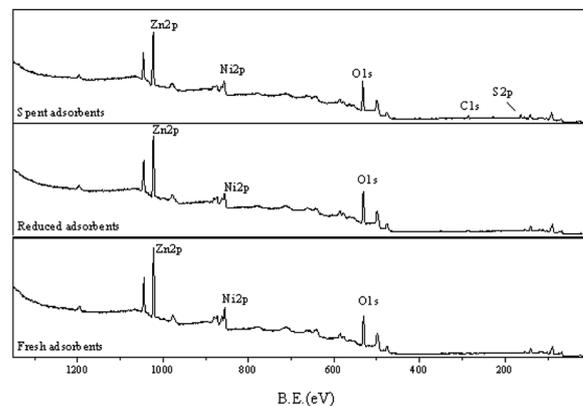| Sample	D (%)	SA$_{Ni}$ (m^2 g^{-1})	MCS (nm)
Adsorbent	0.0236	0.1568	3582.4852

Fig. 6 XPS spectra of fresh, reduced and spent adsorbent.

Table 3 presents that the specific surface area is about 149 m^2 g^{-1}, and pore diameter is about 5.90 nm. It means the sorbents have a big specific surface area, and the pore diameter distribution is large enough for the adsorption of sulfur components, even refractory sulfur compounds like benzo-thiophene (BT).

Dispersion of Ni component

To detect Ni dispersion, the hydrogen and oxygen pulse titration method is used. Table 4 shows the bulk metal dispersion (D), specific surface area (SANi) and metal crystal size (MCS) of Ni component in fresh sorbents. It can be seen that Ni component in adsorbent is difficult to be reduced after hydrogen and oxygen pulse titration, and the bulk metal dispersity is only about 0.02%. Based on the above data, the Ni element on the sorbent surface mostly exists in the form of NiO.

XPS results

XPS spectra is used to characterize fresh, reduced and spent adsorbents, shown in Fig. 6. All XPS spectra were calibrated using the C 1s peak at 285.4 eV. From Fig. 6, Zn, Ni and S elements are at 2p energy level. After the desulfurization, S and C elements can be detected on the adsorbent surface. It indicates that S elements are adsorbed and carbon deposits are formed on the surface of the adsorbents.
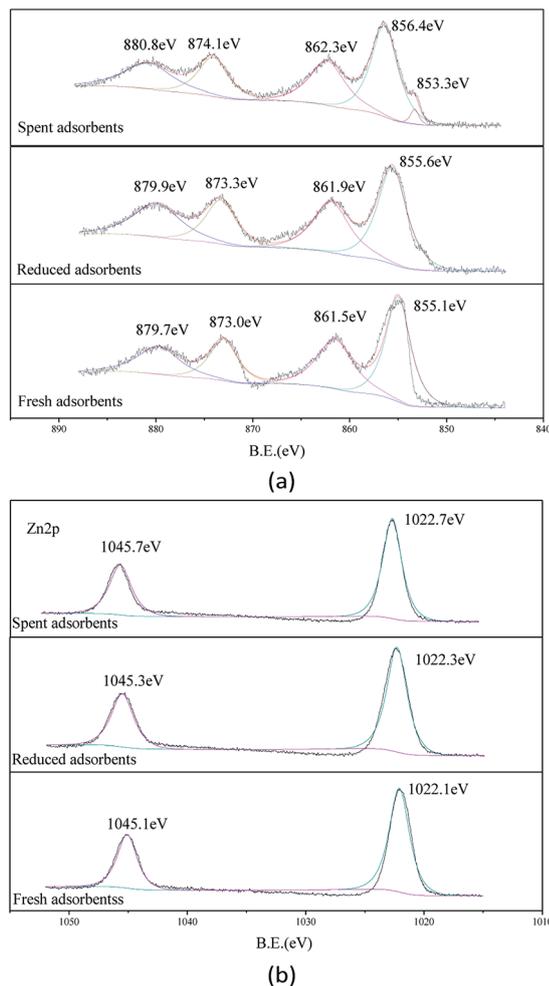
Fig. 7 XPS spectra of Ni and Zn elements (a) Ni, (b) Zn.

Fig. 8 TEM of fresh and reduced NiO/ZnO−Al$_2$O$_3$−SiO$_2$ adsorbents (a) fresh, (b) after reduction.

of Zn 2p increases a little, indicating that sulfur atom reacts with ZnO to form ZnS. Furthermore, for S 2p spectra (Fig. 6), the peak at 162.4 eV is attributed to ZnS group, also indic-ating sulfur atom transfers to ZnS from ZnO.

TEM results

Fig. 8 illustrates the TEM photos of fresh and reduced adsorbents. For the fresh adsorbent, the spots in a diameter range close to 4 nm are NiO components, which are evenly dispersed on the supporter surface. The crystal lattice of adsorbent distributes in the shape of stripe, which may be caused by the preparation method. The striped crystal lattice may be formed by the supporter Al$_2$O$_3$ and SiO$_2$. From the Fig. 8(b), after reduction process at 600 °C reduction temperature, the diameters of the black spots increase to 14 nm and the stripes become more visible and darker. Under high reduction temperature, it would lead to a certain degree of sintering of the adsorbent. Due to the strong interactions between NiO and the

XPS spectra of Ni and Zn are presented in Fig. 7. Normally, Ni XPS spectra of Ni-bearing compounds consist of a main photo-peak and an associated satellite peak located at 6 to 8 eV higher binding energy than the main peak. Fig. 7(a) presents Ni 2p$_{3/2}$ photo-peaks of the Ni compounds. In the figure, the Ni 2p$_{3/2}$ spectrum 852.5 (±0.2) eV of Ni metal was not observed for the three adsorbents.[32] This indicates that NiO cannot be reduced by hydrogen pretreatment. Peaks of 855.1 eV and 861.5 eV of the fresh adsorbents are attributed to the main peak and the satellite peak of the Ni 2p$_{3/2}$ spectra of NiO, respectively. The peaks centered at bind energy of 873.0 eV and 879.7 eV are attributed to Ni 2p$_{1/2}$ spectra of NiO.[33] In the XPS spectra of the spent adsorbent, a peak at bind energy 853.3 eV appears after desulfurization. This is the main peak of Ni 2p$_{3/2}$ in NiS. Besides, small increments of binding energy of Ni 2p$_{3/2}$ photo-peaks were observed for the reduced adsorbent and the spent adsorbent. This suggests that the chemical interaction between NiO and the support ZnO−Al$_2$O$_3$−SiO$_2$ is enhanced.

Fig. 7(b) shows the Zn 2p spectra of various adsorbents. The peak centered at bind energy of 1022.1 eV in fresh adsorb-ent is assigned to Zn 2p$_{3/2}$, and the peak at bind energy of 1045.25 eV is attributed to Zn 2p$_{1/2}$. After desulfurization, the bind energy
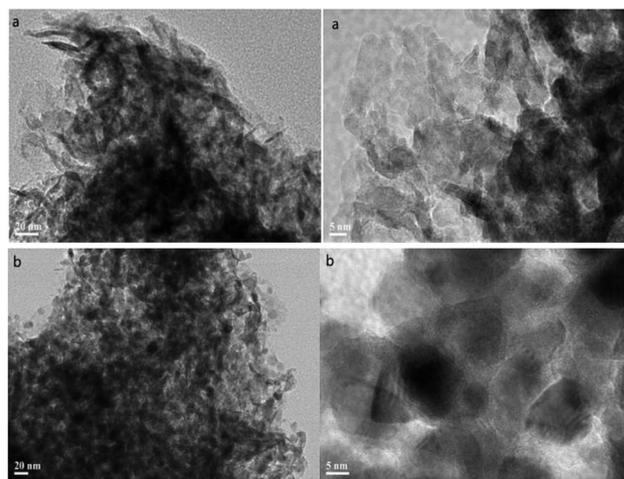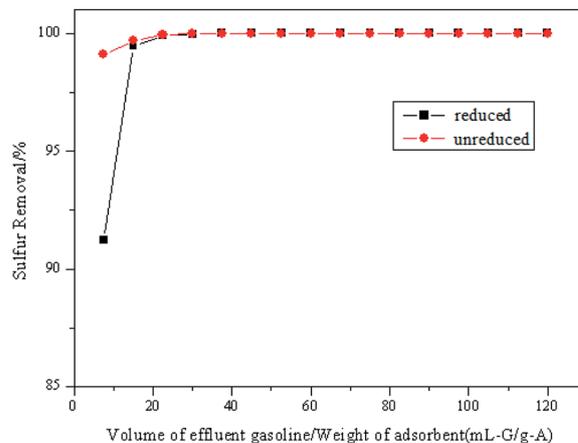

Fig. 9 Effect of hydrogen pretreatment on desulfurization performance of adsorbents.

support, the NiO components are agglomerated to some extent and the alloy Al–Ni are formed. These stripes include the crystalline phases of $AlNi_3$, SiO_2, ZnO and NiO. Compared with the fresh sorbent, the phases have been crystallized again. Distinction between these grains is more obvious.

Effect of hydrogen pretreatment on desulfurization

Fig. 9 shows the different desulfurization performance of the reduced and unreduced adsorbents. The sulfur content of the FCC gasoline feed is 243.48 $\mu g\ g^{-1}$. It is interesting to see that the desulfurization capacity of unreduced sorbent is higher than that of the reduced sorbent at the beginning of desulfurization process. The reduced sorbent does not give a better desulfurization performance at the starting point. The formation of Ni–Al or Ni–Zn alloy, after hydrogen pretreatment, is perhaps the main reason behind this phenomenon.[19] After the point of 20 mL-G, the reduced and unreduced sorbents all show good desulfurization performance and keep a high desulfurization level. This indicates that hydrogen pretreatment decreases the activity of desulfurization of the sorbent and leads the active component NiO agglomerated, even to form Ni–Al alloy. With the desulfurization capacity increasing, the alloy will be separated to active NiO and ZnO components, and then the sorbents achieve high desulfurization capacity.[19]

The above analysis demonstrates that NiO is hard to be reduced to Ni^0 by hydrogen pretreatment. Also, NiO/ZnO–Al_2O_3–SiO_2 adsorbent without hydrogen pretreatment performs a better desulfurization than the adsorbent after hydrogen pretreatment. It means hydrogen pretreatment is not necessary for RADS process. NiO and Ni^0 show a good synergistic desulfurization ability as the active components in the desulfurization process. Apparently, the mechanism of desulfurization on NiO is different from that on Ni. The mechanism of desulfurization on NiO/ZnO–Al_2O_3–SiO_2 adsorbent needs to be further discussed.

Mechanism of desulfurization on NiO/ZnO–Al_2O_3–SiO_2 adsorbent

According to the reports of Babich *et al.* and Huang *et al.*, the reactive mechanism of desulfurization on Ni/ZnO adsorbent can be concluded as follows: Firstly, thiophene can be adsorbed onto the reduced Ni sites, then the C–S bond ruptures to form Ni_3S_2 and C_4 olefins, which is released back into the stream. After that, the sulfur is transferred from Ni_3S_2 to H_2S in the presence of hydrogen, then H_2S is accepted by ZnO to form ZnS. Finally, the Ni sites can participate in the adsorption of sulfur atoms again.[9,34]

Based on the above mechanism, reduced Ni is considered as the main active component, but it probably ignores the fact that NiO could directly react with thiophene compound. On the basis of the testing results in this work, a small change of the RADS mechanism is proposed and shown in Fig. 10. In this mechanism, firstly, the sulfur atoms from thiophene molecules is attached to the surface NiO molecules through a reaction which leads to the formation of NiS. This new reaction is proved by the H_2-TPR results and the desulfurization performance
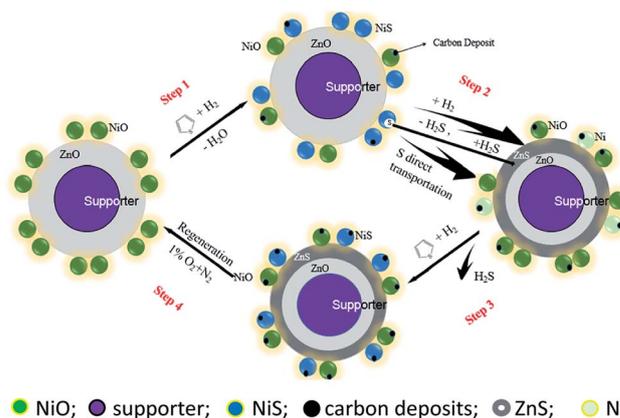

Fig. 10 The possible reaction mechanism of desulfurization on NiO/ZnO–Al_2O_3–SiO_2.

shown in Fig. 9. The next step will form Ni^0 in that a certain proportion of NiS could be reduced. Besides, a direct transportation of sulfur from NiS to ZnO probably happened, which directly form NiO and ZnS. The conversion of ZnO to ZnS is progress-ed by both the latter reaction and the immobilization of H_2S releas-ed by the reduction of NiS. After that, with the existence of metallic nickel, along with nickel oxide, further feed of thiophene is treated not only in the way described in step 1 but also through the reaction of Ni^0.

Theoretically, desulfurization will continue till all ZnO species contained in adsorbents have been converted to ZnS. If the actual situation is taken into account, it should not be ignored that carbon deposits accumulate on the surface as the reaction goes on, which may strongly prevent the progressing of the significant step 2. After being placed in the mixed gas of 1% oxygen and 99% nitrogen at a certain temperature for a few hours listed in Table 2, carbon deposits on used adsorbents can be burned out.[23] Usually those regenerated sorbents can serve as relatively fresh adsorbents to participate in desulfurization continuously.

Conclusions

The effect of hydrogen pretreatment for NiO/ZnO–Al_2O_3–SiO_2 adsorbent is discussed in this work. XRD results showed that NiO is difficult to be reduced to Ni^0 after hydrogen pretreatment at 440 °C reduction temperature. Combined with TPR results, high sintering temperature of the prepared adsorbent increases the reduction tempe-rature of NiO. The desulfurization performance showed that NiO/ZnO–Al_2O_3–SiO_2 adsorbent without hydrogen pretreatment performed a better desulfurization than the adsorbent after hydrogen pretreatment at the beginning of desulfurization process. On the basis of the testing and RADS results, we assumed that NiO and metallic Ni could perform as the main active components together. Some change of the Babichet's RADS mechanism was proposed. First, the sulfur atoms from thiophene molecules could be attached to the surface NiO molecules to form NiS. Second, a direct transportation of sulfur from NiS to ZnO probably happened, which directly forms NiO and ZnS.

Conflicts of interest

There are no conflicts to declare.

Acknowledgements

Notes and references

1 J. H. Kim, X. Ma, A. Zhou and C. Song, *Catal. Today*, 2006, **111**, 74–83.

2 H. J. Jeon, H. K. Chang, S. H. Kim and J. N. Kim, *Energy Fuels*, 2009, **23**, 2537–2543.

3 J. Xiao, Z. Li, B. Liu, Q. Xia and M. Yu, *Energy Fuels*, 2008, **22**, 3858–3863.

4 G. P. Khare, *US Pat.*, 6 531 053, 2003.

5 G. P. Khare, *US Pat.*, 6 184 176, 2001.

6 U. T. Turaga and J. J. Gislason, *US Pat.*, 7 201 839, 2007.

7 S. Brunet, D. Mey, G. Pérot, C. Bouchy and F. Diehl, *Appl. Catal., A*, 2005, **278**, 143–172.

8 K. Tawara, T. Nishimura, H. Iwanami and T. Hasuike, *J. Energy Chem.*, 2001, **40**, 2367–2370.

9 I. V. Babich and J. A. Moulijn, *Fuel*, 2003, **82**, 607–631.

10 W. Xu, C. Xiong, G. Zhou and H. Zhou, *Acta Pet. Sin.*, 2008, **24**, 739–743.

11 T. Wang, X. Wang, Y. Gao, Y. Su, Z. Miao, C. Wang, L. Lu, L. Chou and X. Gao, *J. Energy Chem.*, 2015, **24**, 503–511.

12 J. Fan, W. Gang, S. Yu, C. Xu, H. Zhou, G. Zhou and J. Gao, *Ind. Eng. Chem. Res.*, 2010, **49**, 8450–8460.

13 H. Li, L. Dong, L. Zhao and C. Xu, *Ind. Eng. Chem. Res.*, 2017, **56**, 3813–3821.

14 M. T. Timko, J. A. Wang, J. Burgess, P. Kracke, L. Gonzalez, C. Jayee and D. A. Fischere, *Fuel*, 2016, **163**, 223–231.

15 W. Wang, X. Li, Y. Zhang and M. Tang, *Catal. Sci. Technol.*, 2017, **7**, 4413–4421.

16 R. Ullah, P. Bai, P. Wu, Z. Zhang and Z. Zhong, *Energy Fuels*, 2016, **30**, 2874–2881.

17 M. Moradi, R. Karimzadeh and E. S. Moosavi, *Fuel*, 2018, **217**, 467–477.

18 I. Bezverkhyy, O. V. Safonova, P. Afanasiev and J. P. Bellat, *J. Phys. Chem. C*, 2009, **113**, 17064–17069.

19 A. Ryzhikov, I. Bezverkhyy and J. P. Bellat, *Appl. Catal., B*, 2008, **84**, 766–772.

20 Y. Zhang, Y. Yang, H. Han, M. Yang, L. Wang, Y. Zhang, Z. Jiang and C. Li, *Appl. Catal., B*, 2012, **21**, 13–19.

21 A. Ochoa, B. Aramburu, B. Valle, D. Resasco, J. Bilbao, A. Gayubo and P. Castaño, *Green Chem.*, 2017, **19**, 4315–4333.

22 J. Tapia, N. Acelas, D. López and A. Moreno, *Univ. Sci.*, 2017, **22**, 71–85.

23 F. Ju, C. Liu, C. Meng, S. Gao and H. Ling, *Energy Fuels*, 2015, **29**, 6057–6067.

24 F. Ju, C. Liu, K. Li, C. Meng, S. Gao and H. Ling, *Energy Fuels*, 2016, **30**, 6688–6697.

25 H. Kim, K. Jun, S. Kim, H. Potdar and Y. Yoon, *Energy Fuels*, 2006, **20**, 2170–2173.

26 K. Jun, W. Shen, R. Rama and K. Lee, *Appl. Catal., A*, 1998, **174**, 231–238.

27 X. An, B. Wu, W. Hou, H. Wan, Z. Tao and T. Li, *J. Mol. Catal. A: Chem.*, 2007, **263**, 266–272.

28 A. A. Mirzaei, H. R. Shaterian, R. W. Joyner, M. Stockenhuber, S. H. Taylor and G. J. Hutchings, *Catal. Commun.*, 2003, **4**, 17–20.

29 P. Magnoux, P. Cartraud, S. Mignard and M. Guisnet, *J. Catal.*, 1987, **106**, 235–241.

30 S. F. Rahbar, F. Meshkani and M. Rezaei, *Ultrason. Sonochem.*, 2017, **34**, 436–447.

31 J. D. Seader and E. J. Henley, *Separation Process Principles*, New York, Wiley, 1998.

32 G. Ertl, R. Hierl, H. Knözinger, N. Thiele and H. P. Urbach, *Appl. Surf. Sci.*, 1980, **5**, 49–64.

33 H. W. Nesbitt, D. Legrand and G. M. Bancroft, *Phys. Chem. Miner.*, 2000, **27**, 357–366.

34 L. C. Huang, G. F. Wang, Z. F. Qin, M. X. Du, M. Dong, H. Ge, Z. W. Wu, Y. D. Zhao, C. Y. Ma, T. D. Hu and J. G. Wang, *Catal. Commun.*, 2010, **11**, 592–596.